Evaluation and Comparison of the IRS-P6 and the Landsat Sensors

Gyanesh Chander, *Member, IEEE*, Michael J. Coan, and Pasquale L. Scaramuzza

***Abstract*—The Indian Remote Sensing Satellite (IRS-P6), also called ResourceSat-1, was launched in a polar sun-synchronous orbit on October 17, 2003. It carries three sensors: the high-resolution Linear Imaging Self-Scanner (LISS-IV), the medium-resolution Linear Imaging Self-Scanner (LISS-III), and the Advanced Wide-Field Sensor (AWiFS). These three sensors provide images of different resolutions and coverage. To understand the absolute radiometric calibration accuracy of IRS-P6 AWiFS and LISS-III sensors, image pairs from these sensors were compared to images from the Landsat-5 Thematic Mapper (TM) and Landsat-7 Enhanced TM Plus (ETM+) sensors. The approach involves calibration of surface observations based on image statistics from areas observed nearly simultaneously by the two sensors. This paper also evaluated the viability of data from these next-generation imagers for use in creating three National Land Cover Dataset (NLCD) products: land cover, percent tree canopy, and percent impervious surface. Individual products were consistent with previous studies but had slightly lower overall accuracies as compared to data from the Landsat sensors.**

***Index Terms*—Advanced Wide-Field Sensor (AWiFS), calibration, canopy, characterization, Enhanced Thematic Mapper Plus (ETM+), impervious, Indian Remote Sensing Satellite (IRS-P6), land cover, Landsat, medium-resolution Linear Imaging Self-Scanner (LISS-III), reflectance, ResourceSat-1, spectral bands.**

I. Introduction

DETECTION and quantification of change in the Earth's environment depends on satellites that can provide calibrated consistent measurements of the Earth's surface features. The Landsat program began in 1972 and since then has provided continuous consistent measurements of the Earth's surface features over seven mission generations. To date, the Landsat suite of satellites has collected the longest continuous archive of multispectral data of any space program. Landsat-5 (L5) and Landsat-7 (L7) are the two currently operational satellites in the Landsat series. The Indian Remote Sensing Satellites (IRS) constellation program consists of three currently operating satellites: IRS-P6 (ResourceSat-1), IRS-1C, and IRS-1D. Section I-B provides an overview of these sensors.

Manuscript received May 9, 2007; revised July 18, 2007. This work was supported by the U.S. Geological Survey (USGS) Land Remote Sensing (LRS) Program and the Remote Sensing Technologies (RST) Project within LRS under USGS Contract 03CRCN0001.

The authors are with the Science Application International Corporation (SAIC), San Diego, CA, contractor to the U.S. Geological Survey (USGS) Center for Earth Resource Observation and Science (EROS), Sioux Falls, SD 57198 USA (e-mail: gchander@usgs.gov).

Color versions of one or more of the figures in this paper are available online at http://ieeexplore.ieee.org.

Digital Object Identifier 10.1109/TGRS.2007.907426

A. Purpose of This Paper

This paper evaluates and compares the IRS-P6 and the Landsat sensors and includes as follows: 1) an overview of the sensors; 2) a comparison of the relative spectral response (RSR) profiles; 3) calibration by near-simultaneous surface observations; and 4) preliminary assessments of the utility of IRS-P6 imagery for production of National Land Cover Dataset (NLCD) products.

B. Sensor Overview

The section below provides an overview of the sensors that were used in this paper.

1) L5 Thematic Mapper (TM): The L5 TM is an Earth-imaging sensor that was launched on March 1, 1984. It incorporated advancements in spectral, radiometric, and geometric capabilities relative to the multispectral scanner flown on previous Landsat satellites. L5 TM bands 1–5 and 7 have 16 detectors with center wavelengths of approximately 0.49, 0.56, 0.66, 0.83, 1.67, and 2.24 μm, respectively [1]. The detectors for bands 1–4 are located at the primary focal plane, where the temperature is not controlled but normally varies between 292 and 300 K. The detectors for bands 5–7 are located at the cold focal plane (CFP). Because of their relatively long wavelengths, high noise signals result from the internal thermal excitation of the detector materials. To minimize this noise and allow adequate detection of scene energy, a radiative cooler maintains the CFP temperature at set points between 95 and 105 K. The internal calibrator (IC) is incorporated as an onboard radiometric calibration system for the L5 TM. Onboard calibration of the TM uses lamps to calibrate the reflective bands and a blackbody source to calibrate the thermal band.

2) L7 Enhanced TM Plus (ETM+): The ETM+ sensor was launched on April 15, 1999, on the L7 platform; it is based on the TM sensors onboard the Landsat-4 and L5 satellites. The L7 ETM+ sensor added a new panchromatic band, improved spatial resolution of the thermal band to 60 m, and added two calibration devices to help improve the radiometric calibration. L7 ETM+ has three onboard calibration devices: a full-aperture solar calibrator, which is a white painted diffuser panel; a partial aperture solar calibrator, which is a set of optics that allows the L7 ETM+ to image the Sun through small holes; and an IC, which consists of two lamps, a black body, a shutter, and optics to transfer the energy from the calibration sources to the focal plane. One of the requirements of the L7 mission is to achieve radiometric calibration accuracy of the ETM+ data with an uncertainty of less than 5% in at-sensor radiance [1],

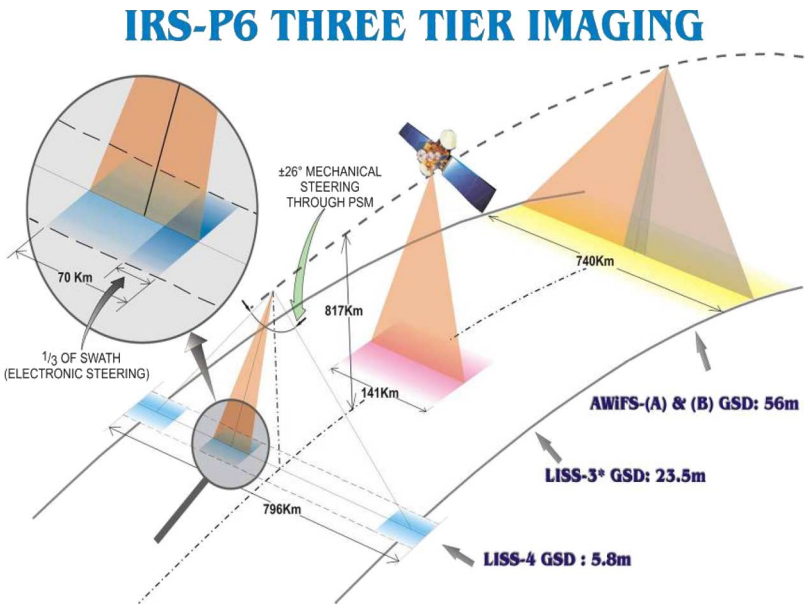

Fig. 1. P6 sensors swath covered on the ground [4].

a requirement more stringent than in the past for the Landsat program.

Another significant improvement in the L7 system is the incorporation of an image-assessment system (IAS) as part of the ground processing system at the U.S. Geological Survey, Center for Earth Resources Observation and Science, Sioux Falls, SD. IAS analysts work with their counterparts at the Landsat Project Science Office of the National Aeronautics and Space Administration's Goddard Space Flight Center to analyze the calibration information and update the algorithms used within the IAS. The IAS is responsible for offline assessment of image quality to ensure compliance with the radiometric and geometric requirements of the L7 spacecraft and the ETM+ sensor throughout the Landsat mission. One of the most important roles of the IAS is the generation of the calibration-parameter file, which contains all of the necessary parameters for generating a geometrically and radiometrically calibrated product. In early 2002, the IAS also became responsible for the routine radiometric and geometric calibration of the L5 TM following its transition to bumper-mode operations.

3) IRS-P6 Advanced Wide-Field Sensor (AWiFS) and Medium-Resolution Linear Imaging Self-Scanner (LISS-III): IRS-P6 is also called ResourceSat-1. The IRS-P6 is a three-axis body-stabilized satellite. Launched on October 17, 2003, it has an operational life of five years, with a near-polar sun-synchronous orbit at a mean altitude of 817 km. The IRS-P6 payload consists of three sensors: LISS-III, AWiFS, and a high-resolution multispectral sensor (LISS-IV). All three sensors work on the "pushbroom scanning" concept, using linear arrays of detectors. In this mode of operation, each line of image data is electronically scanned, and contiguous lines are imaged by the forward motion of the satellite. Unique to IRS-P6 is that three sensors with different resolutions and swath widths are on the same platform, as shown in Fig. 1. [2]–[4].

Medium-Resolution Linear Imaging Self-Scanner (LISS-III): The P6 LISS-III is a multispectral sensor operating in four spectral bands, three in the visible and near-infrared (VNIR) bands and one in the short-wavelength infrared (SWIR) region, with 23.5-m spatial resolution and a ground swath of 141 km. The P6 LISS-III sensor is a nadir-looking sensor with a 24-day revisit cycle [2]. A field of light-emitting diodes (LEDs)—four in the visible bands and six for the SWIR bands—are used as calibration sources, allowing a cycle of six nonzero intensity levels during the acquisition of dark data.

Advanced Wide-Field Sensor (AWIFS): The P6 AWiFS camera operates in four spectral bands similar to P6 LISS-III, providing a spatial resolution of 56 m at nadir and covering a ground swath of 740 km. To cover this wide swath, the P6 AWiFS camera is split into two separate electrooptic modules, AWiFS-A and AWiFS-B, as shown in Fig. 2. [2]. P6 AWiFS has an LED-based calibration source similar to P6 LISS-III but with six LEDs and 16 nonzero intensity levels available.

C. RSR Profiles

Figs. 3 and 4 show the RSR profiles between corresponding L7 ETM+, L5 TM, and P6 AWiFS and LISS-III spectral bands. Table I summarizes the spectral range of these sensors. The L7 ETM+ bands were based on the seven L5 TM spectral bands. The P6 AWiFS and LISS-III bands 2–5 are similar to the corresponding L5 TM and L7 ETM+ spectral bands.

D. L7 ETM+, L5 TM, P6 AWIFS, and P6 LISS-III Quantization

The data quantization for L7 ETM+ and L5 TM is 8 bits. L7 employs two alternate gains that permit enhanced radiometric resolution in the high-gain mode and expanded dynamic range in the low-gain mode. Geometrically and radiometrically calibrated products, known as Level 1G products, are only

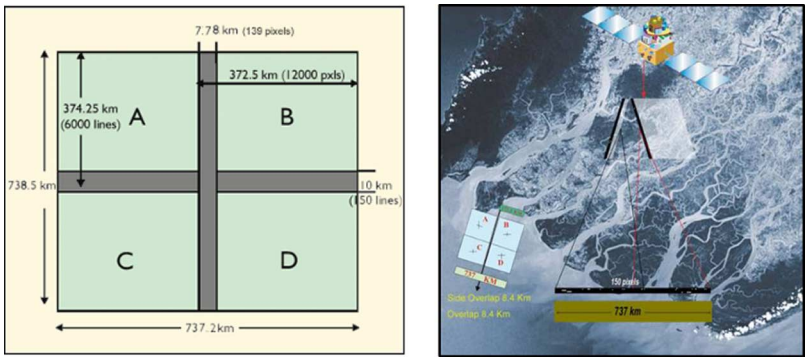

Fig. 2. P6 AWiFS twin cameras [4].

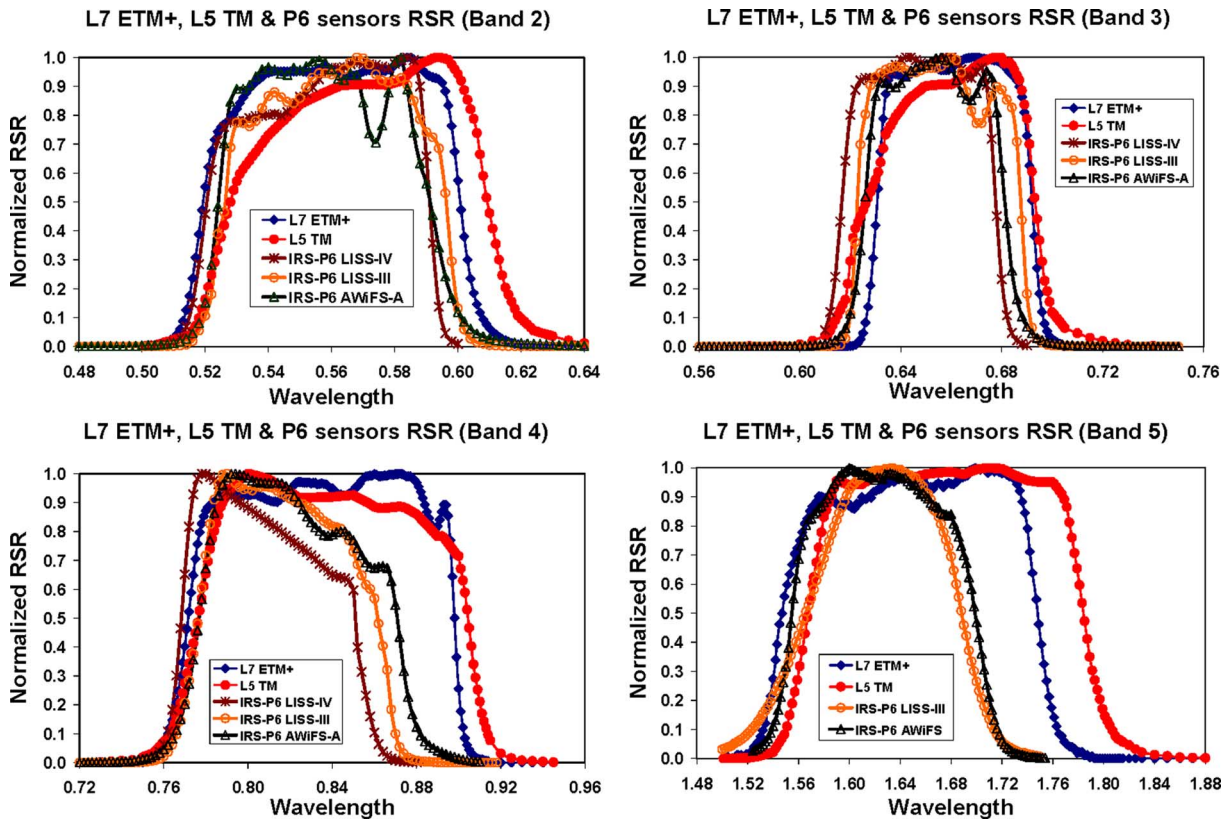

Fig. 3. RSR profiles of L7 ETM+, L5 TM, P6 AWiFS, and P6 LISS-III sensors.

available as 8-bit images for Landsat sensors. The radiometric resolution of the IRS-P6 sensors varies.

1) P6 AWiFS has 10 bits.
2) P6 LISS-III (VNIR) has 7 bits with four gain settings.
3) P6 LISS-III (SWIR) has 7 out of 10 bits (sliding).

The analog-to-digital (A/D) converter is 12 bits for P6 AWiFS and P6 LISS-III SWIR. The data are captured as 12 bits, and the two least significant bits are ignored. The P6 AWIFS data corresponding to all four bands are received as 10-bit parallel data. For the P6 LISS-III SWIR bands, the selected seven consecutive bits out of 10 bits generated at payload end are transmitted. The selection of 7 bits for the SWIR band is done by bit sliding in the baseband-data-handling system formatter. In the formatter, any consecutive 7 bits out of 10 bits are selected by a data command before multiplexing the data. The A/D converter is 7 bits for P6 LISS-III VNIR bands. The data are captured and transmitted as 7 bits with four pregain setting options.

The level-1 product for P6 LISS-III is available as 8-bit images. P6 AWiFS data products are available as 8- and 10-bit images.

II. Data-Set and Test-Site Evaluations

A. Sun-Synchronous Orbits

The L5 and L7 satellites operate in a repetitive, circular, sun-synchronous, and near-polar orbit, with an inclination of 98.2°, at a nominal altitude of 705 km (438 mi) at the Equator. The sun-synchronous orbit means that all acquisitions over a given area occur at the same time of the day. The equatorial crossing

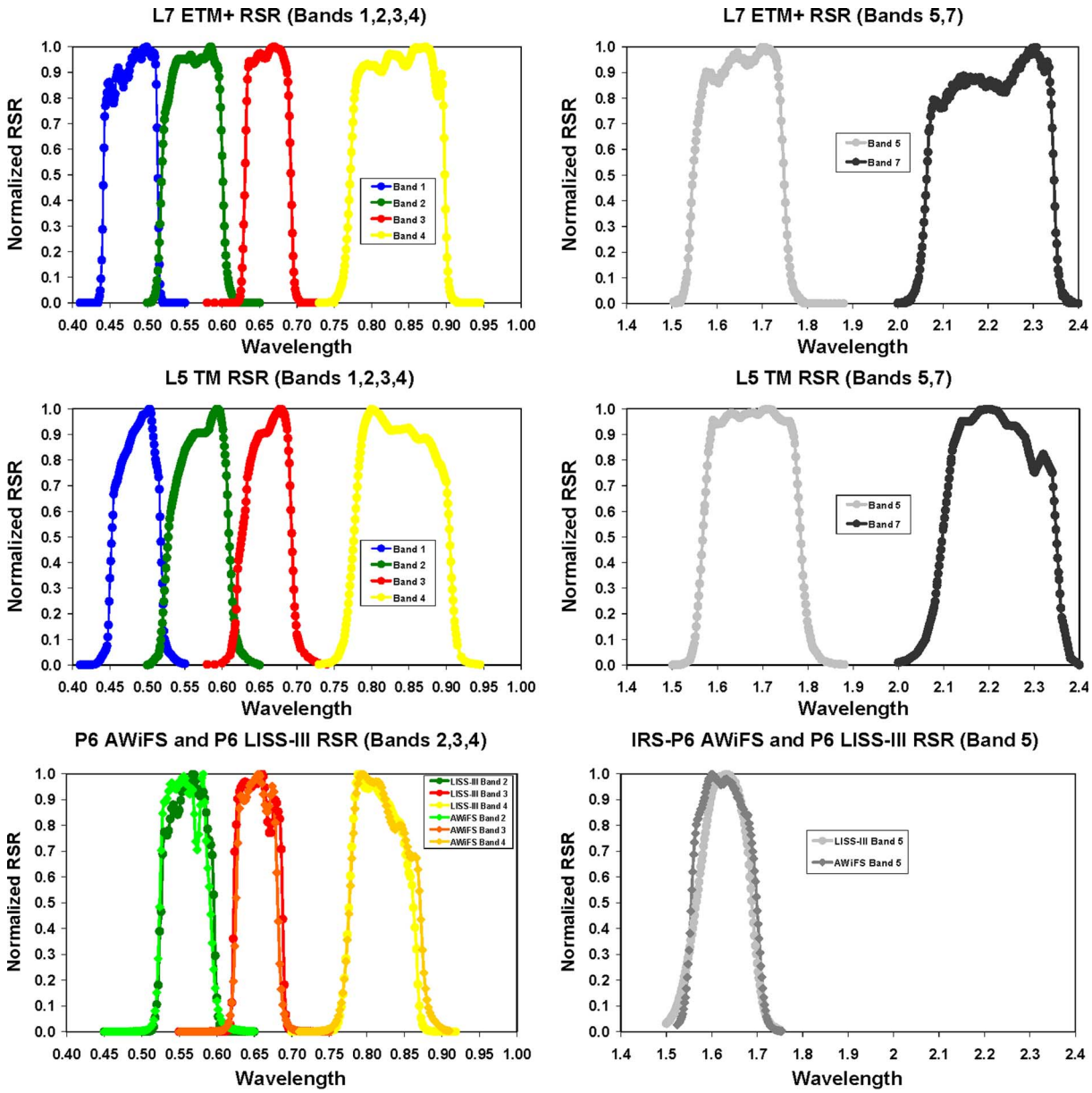

Fig. 4. Comparison of the RSR profiles of L7 ETM+, L5 TM, P6 AWiFS, and P6 LISS-III sensors.

TABLE I
SPECTRAL COVERAGE [1], [2]

	Spectral Range (μm)		
Band	L5 TM	L7 ETM+	P6 AWiFS/LISS-III
1	0.450-0.520	0.450-0.515	
2	0.520-0.600	0.525-0.605	0.52-0.59
3	0.630-0.690	0.630-0.690	0.62-0.68
4	0.760-0.900	0.775-0.900	0.77-0.86
5	1.550-1.750	1.550-1.750	1.55-1.70
6	10.40-12.50	10.40-12.50	
7	2.080-2.350	2.090-2.350	
Pan		0.520-0.900	

time during descending passes (descending passes are on the sunlit side of the Earth and ascending passes are on the dark side of the orbit) is nominally between 9:30 and 10:00 A.M. local time for all Landsat missions. Circling the Earth at 7.5 km/s, each orbit takes nearly 99 min. The spacecraft completes just over 14 orbits per day, covering the entire Earth between 81° north and south latitude every 16 days, completing 233 orbits per cycle on the World Reference System-2 (WRS-2).

The IRS-P6 satellite operates in a circular sun-synchronous near-polar orbit with an inclination of 98.69°, at an altitude of 817 km. The satellite takes 101.35 min to complete 1 rev around the Earth and completes about 14 orbits per day with a ground-track velocity of 6.65 km/s. The entire Earth is covered by 341 orbits during a 24-day cycle.

B. Test-Site Descriptions

Because the number of coincident image pairs between these sensors is limited, the scene selection for these studies proved to be a challenge. Owing to the lack of near-simultaneous images available over the well-characterized and traditionally used calibration- and application-evaluation sites, alternate sites

TABLE II
COINCIDENT P6 AND LANDSAT SCENES USED FOR THIS PAPER

Sensor	Product ID	Path	Row	Time (GMT)	Solar Elevation
Location: Mesa, AZ (June 29, 2005)					
Landsat 7 ETM+	L71036035_03520050629	36	35	17:46:25	65.21 °
Landsat 7 ETM+	L71036036_03620050629	36	36	17:46:49	65.53 °
Landsat 7 ETM+	L71036037_03720050629	36	37	17:47:13	65.77 °
Landsat 7 ETM+	L71036038_03820050629	36	38	17:47:37	65.94 °
Landsat 7 ETM+	L71036039_03920050629	36	39	17:48:01	66.02 °
AWiFS Quad A	AW257047A001	257	47	18:17:35	69.50 °
AWiFS Quad B	AW257047B001	257	47	18:17:35	72.60 °
AWiFS Quad C	AW257047C001	257	47	18:18:23	70.30 °
AWiFS Quad D	AW257047D001	257	47	18:18:23	73.60 °
LISS-III	L32570470101	257	47	18:18:14	71.48 °
Location: Salt Lake City, UT (June 19, 2005)					
Landsat 5 TM	LT5038030000517010	38	30	17:54:58	62.95 °
Landsat 5 TM	LT5038031000517010	38	31	17:55:22	63.59 °
Landsat 5 TM	LT5038032000517010	38	32	17:55:46	64.18 °
AWiFS Quad A	000010491201	255	40	18:23:45	65.50 °
AWiFS Quad B	000010491301	255	40	18:23:45	68.10 °
AWiFS Quad C	000010491401	255	40	18:24:39	67.50 °
AWiFS Quad D	000010491501	255	40	18:24:39	70.30 °
LISS-III	000010491601	255	41	18:24:51	68.64 °

were investigated that have high reflectance, large dynamic range, high spatial uniformity, high sun elevation, and minimal cloud cover. The final scenes selected for this paper were over Mesa, AZ, and Salt Lake City, UT.

1) Mesa, AZ: A cloud-free L7 ETM+ scene was acquired on June 29, 2005. After 31 min, P6 AWiFS and LISS-III scenes covering part of the same footprint were acquired. Because of the scan-gap issue, the prior and post L7 scenes (June 13 and July 15) were also acquired, completing the L7-based data set for the NLCD validation. Mesa is a desert site with little vegetation. The L7 ETM+ scenes are referenced in the WRS-2 with path 36, rows 35–39. The P6 reference is path 257, row 47.
2) Salt Lake City, UT: A cloud-free L5 TM scene was acquired on June 19, 2005. After 31 min, a P6 AWiFS and LISS-III scene of the same region was acquired. The L5 TM scenes are referenced in the WRS-2 system with path 38, rows 30–32. The P6 reference is path 255, row 41.

In both test sites and for each available image source, the area common to all images was evaluated for its ability to duplicate existing NLCD products. Table II lists the coincident P6 and Landsat scenes selected for this paper, along with the location, product ID number, path, row, date of acquisition, and the sun-elevation angle for the scenes. Figs. 5 and 6 show the approximate image boundaries of the scenes used.

C. Data-Processing System

Orthorectified scenes were used for this paper. Terrain correction includes radiometric, geometric, and precision correction, as well as the use of a digital elevation model (DEM) to correct relief displacement caused by local topography. The accuracy of the terrain-corrected product depends on the availability of local ground-control points, as well as the

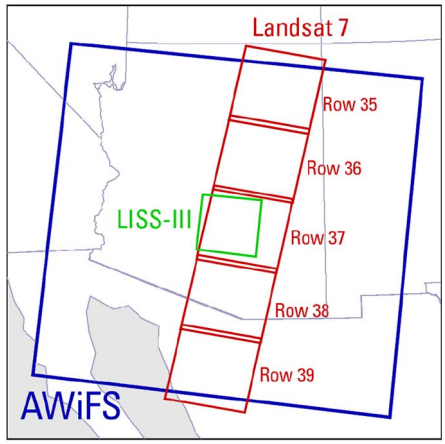

Fig. 5. Image boundaries of scenes used in Mesa, AZ, collection.

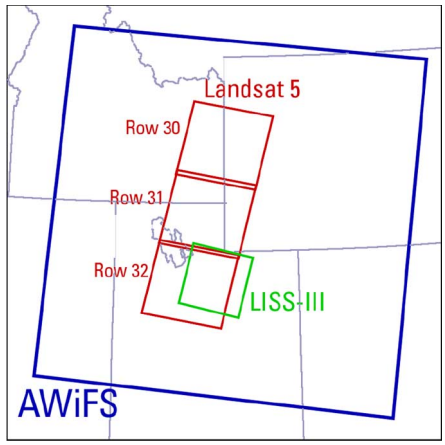

Fig. 6. Image boundaries of scenes used in Salt Lake City, UT, collection.

quality and resolution of the best available DEM. The absolute radiance values are then scaled to calibrated digital numbers (DNs) before being output to the distribution media.

The following processing parameters were used to generate the Landsat products and were chosen to replicate the processing parameters for the P6 AWiFS and LISS-III products as closely as possible.

Map projection	Albers
Standard parallel 1	29.5
Standard parallel 2	45.5
Central meridian	−96
Latitude of origin	23
False northing	0
False easting	0
Horizontal datum	WGS84
Resampling method	cubic convolution
Image orientation	map (north up).

D. Conversion to Reflectance

Remote-sensing satellite detectors exhibit a linear response to incoming radiance, whether from the Earth's surface radiance or internal calibration sources. This response is quantized into 8- or 10-bit values that represent brightness values commonly called DNs. To convert the calibrated DNs to at-aperture

TABLE III
ESUN VALUES USING CHKUR MODTRAN 4.0 SPECTRUM
(IN WATTS PER SQUARE METER TIMES MICROMETERS)

Bands	L5 TM	L7 ETM+	P6 LISS-III	P6 AWiFS
2	1826.000	1840.000	1846.770	1849.820
3	1554.000	1551.000	1575.500	1579.370
4	1036.000	1044.000	1087.340	1075.110
5	215.000	225.700	236.651	235.831

radiance, rescaling gains and biases are created from the known dynamic-range limits of the sensor [5], [6]. This radiance is then converted to top-of-atmosphere (TOA) reflectance by normalizing for solar elevation and solar spectral irradiance. When comparing images from different sensors, there are two advantages in using reflectance instead of radiances. First, the cosine effect of different solar-zenith angles due to the time difference between data acquisitions can be removed, and second, it compensates for different values of the exoatmospheric solar irradiances arising from spectral band differences. Table II lists the solar-elevation angles, and Table III summarizes the solar exoatmospheric spectral irradiances (ESUN) values used in this paper. To maintain consistency with the ETM+, this paper uses spectral-radiance units of watts per square meter times steradian times micrometers.

III. CALIBRATION BY NEAR-SIMULTANEOUS SURFACE OBSERVATIONS

Data continuity requires consistency in the interpretation of image data acquired by different imaging sensors. This section describes the comparisons of the reflectance measurements obtained from the L7 ETM+, L5 TM, and P6 AWiFS and LISS-III sensors.

Cross calibration was performed with image statistics based on large common areas observed near-simultaneously by the two sensors. Because the image acquisitions occurred 31 min apart, it was assumed that the surface and atmospheric conditions did not change during that time. Changes in sun angle were corrected with the conversion to TOA reflectance. A more detailed treatment of the calibration methodology is provided in [7]–[9].

A. Region of Interest (ROI)

The L7, L5, and P6 sensors differ in their along- and across-track pixel sampling. A feature simultaneously observed by these sensors is represented by slightly different numbers of image pixels because of the differences in viewing geometry and sensor scanning times. This makes it very difficult to establish sufficient geometric control to facilitate radiometric comparisons on a point-by-point and/or detector-by-detector basis. Therefore, the analysis approach made use of image statistics based on large homogenous areas common in the image pairs. These large areas were carefully selected using distinct features common to both of the images. Both bright and dark regions were selected to obtain maximum coverage over each sensor's dynamic range, but areas with clouds or cloud shadows were excluded. ROIs were defined within these areas for each image triplet (L5 TM or L7 ETM+, P6 AWiFS, and LISS-III). Gaps in the L7 ETM+ data caused by the scan-line corrector anomaly were discarded. Homogeneity of each region was then tested by rejecting any region with a standard deviation of more than ten DNs in any Landsat band. This left 27 regions for the Mesa, AZ, collection and 34 regions for the Salt Lake City, UT, collection.

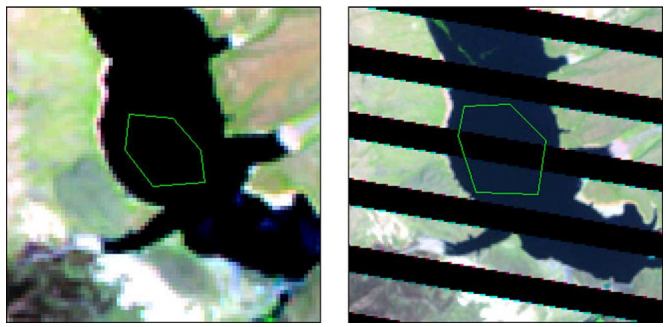

Fig. 7. Paired homogenous ROIs. Data from Mesa, AZ, collection, with (left) P6 AWiFS and (right) L7 ETM+.

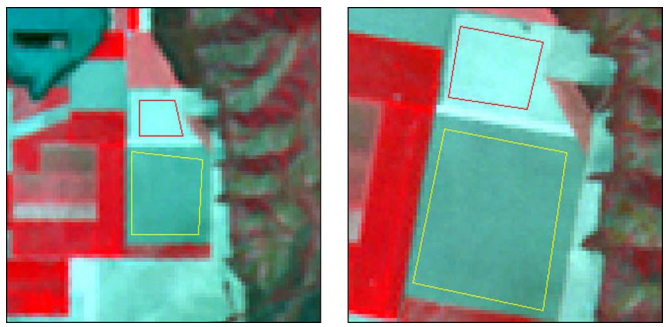

Fig. 8. Paired homogenous ROIs. Data from Salt Lake City, UT, collection, with (left) P6 AWiFS and (right) L5 TM.

Fig. 7 shows a pair of ROIs from the Mesa test site, with AWiFS data on the left and L7 ETM+ data on the right. Fig. 8 shows a pair of ROIs from the Salt Lake City test site, with P6 AWiFS data on the left and L5 TM data on the right.

Once all area ROIs were selected, image statistics were computed to obtain mean and standard-deviation target values on a band-by-band basis. The mean-target statistics were then converted to absolute units of radiance and then to TOA reflectances, taking into account the RSR of the sensor bands and the sun angle during the acquisitions. These reflectance values were then plotted for each sensor pair and a linear fit calculated, giving a relative gain and bias between each sensor pair.

B. Cross-Calibration Results and Discussions

Figs. 9 and 10 show the cross-calibration plots for the Mesa, AZ, collection, and Figs. 11 and 12 show the cross-calibration plots for the Salt Lake City, UT, collection.

As a check of the consistency of the satellite calibrations and the methodology used, a cross calibration was also calculated between the AWiFS and LISS-III sensors. Figs. 13 and 14 show the cross-calibration plots comparing AWiFS reflectances to LISS-III reflectances for the Mesa, AZ, and Salt Lake City, UT, collections, respectively.

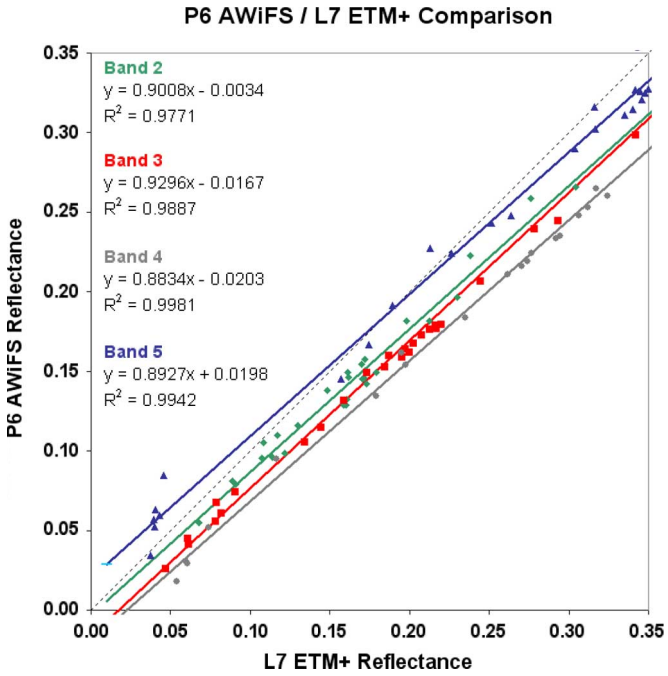

Fig. 9. Reflectance of homogenous regions viewed by the L7 ETM+ plotted against the same regions viewed by P6 AWiFS.

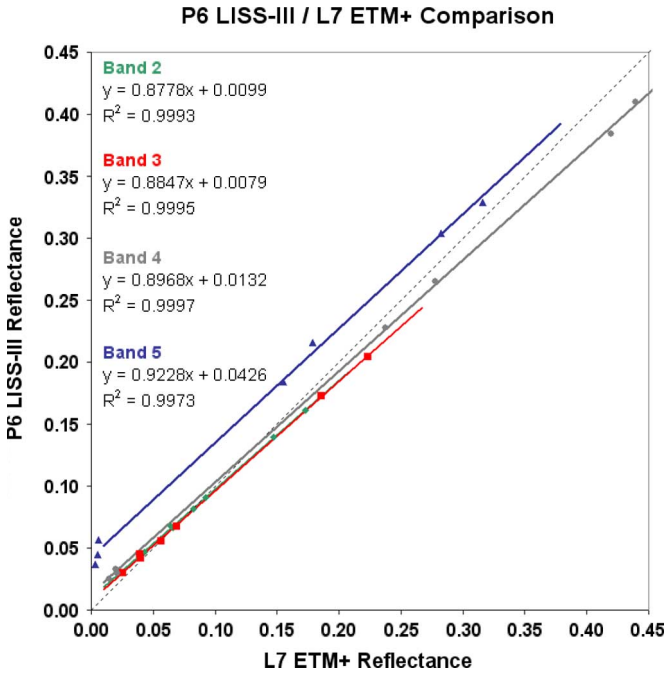

Fig. 10. Reflectance of homogenous regions viewed by the L7 ETM+ plotted against the same regions viewed by P6 LISS-III.

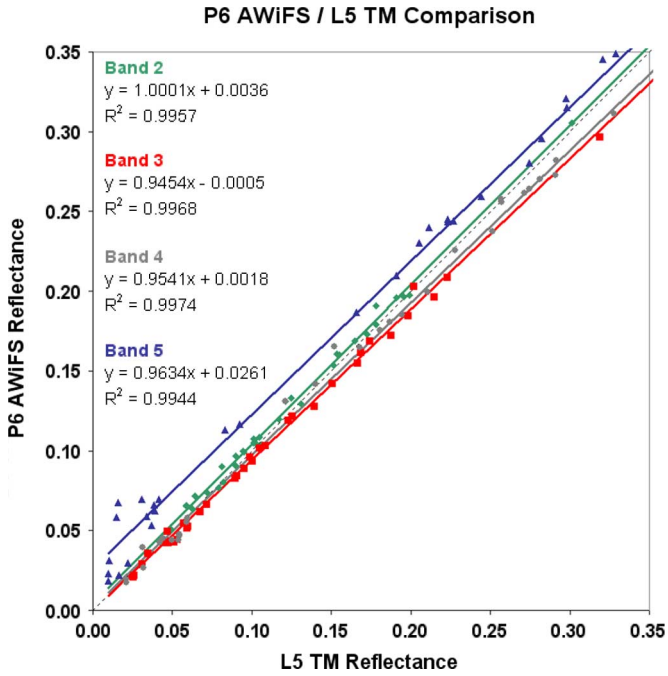

Fig. 11. Reflectance of homogenous regions viewed by the L5 TM plotted against the same regions viewed by P6 AWiFS.

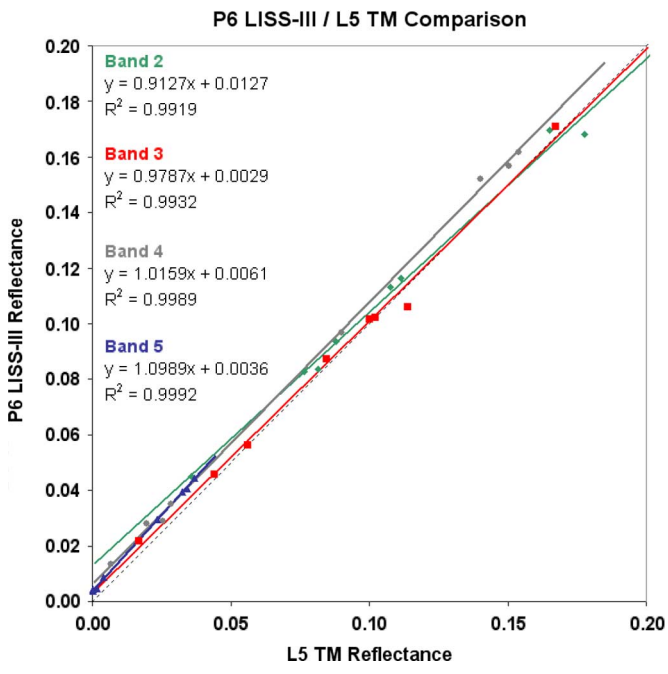

Fig. 12. Reflectance of homogenous regions viewed by the L5 TM plotted against the same regions viewed by P6 LISS-III.

In each set of plots, the reflectance from the Landsat sensor is compared against the reflectance of the AWiFS and LISS-III sensors. The expected 1 : 1 reflectance line is also plotted for reference. A least squares fit has been made to the data in each band, giving the cross-calibration gain and biases as the coefficients of the linear fit.

These preliminary results indicate that the IRS-P6 sensors can be cross calibrated to the Landsat sensors to within an accuracy of 13%. The IRS-P6 AWiFS and LISS-III sensors are within 5.5% of each other in all bands except band 2, which has a 16.4% difference.

Because the AWiFS image was present in both collections and because the calibration of the AWiFS sensor is generally closer to the Landsat sensors than to LISS-III, it is instructive to look at the cross-calibration results as a function of difference from AWiFS. Table IV shows the cross-calibration gains of all four sensors normalized to AWiFS. The cross calibration of AWiFS to the L5 TM produced the best result, with consistent

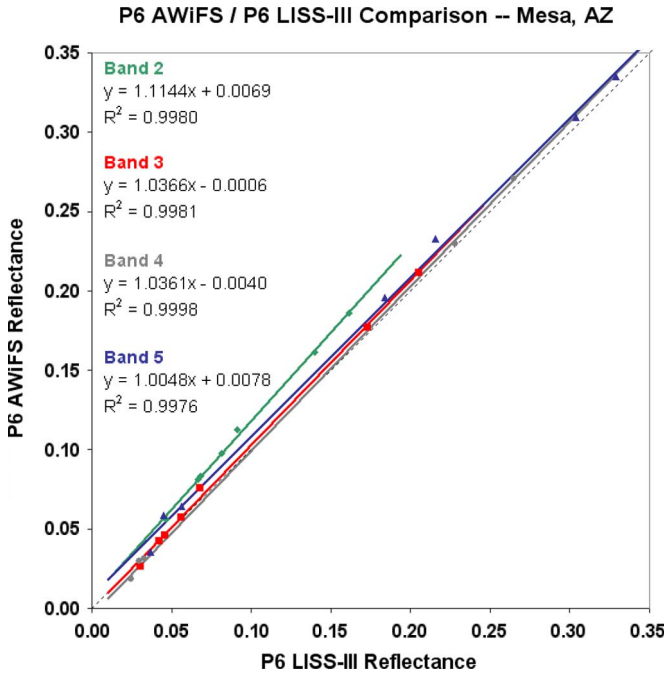

Fig. 13. Reflectance of homogenous regions viewed by both the P6 AWiFS and the P6 LISS-III sensors for the Mesa, AZ, collection.

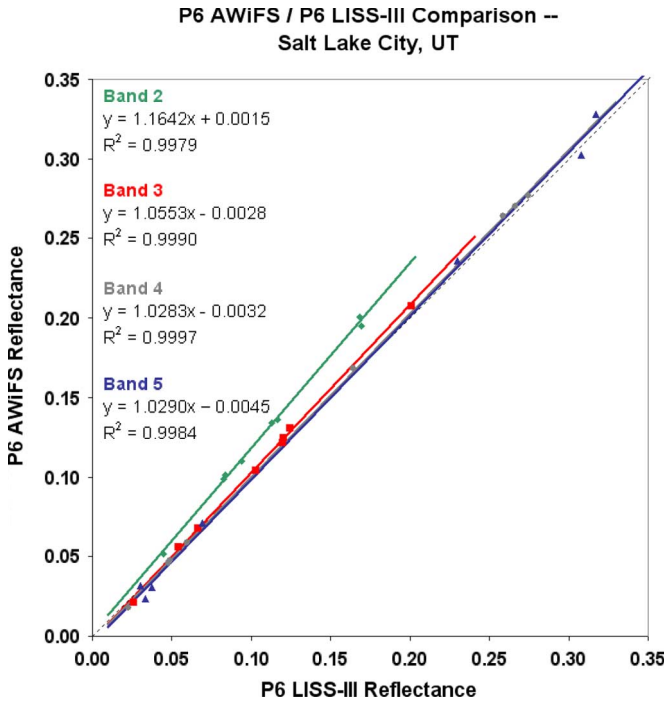

Fig. 14. Reflectance of homogenous regions viewed by both the P6 AWiFS and the P6 LISS-III sensors for the Salt Lake City, UT, collection.

differences in absolute calibration of approximately 6% in all bands of the TM and the AWiFS sensor.

These cross-calibration accuracies should be considered the difference between the Landsat and P6 sensor reflectance data when used for scientific applications. The expected difference in results from those applications—including the NLCD product generation described below—should be similar to the cross-calibration accuracies. This is therefore a preliminary measure

TABLE IV
CROSS-CALIBRATION RESULTS NORMALIZED TO THE AWIFS SENSOR

Sensor	Band			
	2	3	4	5
L5 TM	1.00	1.06	1.05	1.04
L7 ETM+	1.11	1.08	1.13	1.12
P6 AWiFS	*1.00*	*1.00*	*1.00*	*1.00*
P6 LISS-III (Mesa)	0.90	0.96	0.97	1.00
P6 LISS-III (SLC)	0.86	0.95	0.97	0.97

of the viability of using non-Landsat sensors for Landsat data continuity in scientific applications.

A source of error in these results may be in the assumption that the TOA reflectance of all terrain in the study scenes underwent minimal changes between passes of the satellites—a timescale of 30 min. This may not be true for some ROIs, including water regions, croplands in changing wind conditions, and areas near clouds that may have had drastic changes in humidity between satellite passes. As the Landsat TM and ETM+ sensors are known to be calibrated to within 6% of each other [10], [11], the normalized results appear to have a systematic error in the calibration to the ETM+, indicating possible problems in the Mesa, AZ, scene, most likely caused by transient changes in reflectance or aerosol loading.

The RSR of the sensors is also a likely cause of error. Although measured in detail prelaunch, spectral filters are known to degrade postlaunch and are difficult to characterize in orbit. This is the most likely cause of the discrepancy in the cross-calibration between AWiFS and LISS-III in band 2, although it may also affect other bands. Additional work is in progress to characterize the IRS-P6 sensors over the entire mission.

IV. VIABILITY OF IRS-P6 FOR NLCD PRODUCTS

A. NLCD Background

The Multi-Resolution Land Characteristics (MRLC) Consortium is a group of Federal agencies who first joined together in 1993 to purchase L5 imagery for the conterminous U.S. and to develop the NLCD 1992. In 1999, a second-generation MRLC Consortium was formed to purchase three phenologic dates of L7 ETM+ imagery for the entire U.S. (MRLC 2001) and to coordinate the production of a comprehensive land-cover database for the nation called the NLCD 2001.

The MRLC Consortium is designed to meet the current needs of federal agencies for nationally consistent satellite remote-sensing and land-cover data. The consortium also provides imagery and land-cover data as public-domain information, all of which can be accessed through the MRLC website [12].

The NLCD products are raster data layers at 30-m resolution, generated from at least three dates (leaf-off, leaf-on, and spring) of L5 TM and L7 ETM+ imagery. All Landsat imagery is preprocessed with precision terrain corrections and normalized to at-satellite reflectance. The three NLCD 2001 products are land cover, percent tree canopy, and percent impervious surface [13]. Currently, NLCD 2001 has been compiled across all 48 conterminous states. Alaska, Guam, Hawaii, and Puerto Rico are scheduled for completion by December 31, 2007. Methodology and data sources for the next-generation NLCD are being

planned (NLCD 2006 and 2007). Alternative data platforms and providers are being considered to replace the aging L5 and to avoid the current scan-gap problems of L7 ETM+ data.

B. Experimental Design and Procedures

For the NLCD test, the same data were used as in the cross-calibration test except that only one Landsat scene was used for each collection—path 38, row 31 for Salt Lake City, UT, and path 36, row 37 for Mesa, AZ. For the Mesa scene, both the prior and post scenes (June 13 and July 15, respectively) were acquired to make a complete L7-based gap-filled data set.

NLCD classification procedures normally use mosaics of L5 TM and L7 ETM+ imagery from three dates (leaf-off, leaf-on, and spring) capturing phenologic characteristics of the area. Along with ancillary information, the imagery is used in a series of decision-tree regressions [10]. Classifications used standard NLCD tools (ERDAS Imagine, NLCD Mapping Tool, See5, and Cubist) to generate classification logic and map the results. A more detailed explanation of the NLCD products is in [13] and [14].

In both test sites and for each available image source, the area common to all images was evaluated for its ability to duplicate existing NLCD products. Artificial products were constructed by massively sampling existing products and assessing each image source's ability to generate a duplicate by comparing its version to the source. In contrast to the usual NLCD procedures, no ancillary information (e.g., DEM or Slope) was used in the classification. The intent was to generate results based solely on the spectral information unique to each data set.

Owing to different areas of common extent between sensors (P6 AWiFS/Landsat and P6 LISS-III/Landsat) on each test site, two results are reported per available product, per site.

C. Land-Cover Estimation

Land cover is a discrete label based on classification of the Earth's surface as it is represented in imagery. At the time of the experiment, the NLCD 2001 land-cover product for the Salt Lake City site was available but not for the Mesa site. For this reason, land-cover estimations were made only over the Salt Lake City site.

To generate the land-cover training data, 10 000 random points per land-cover class were extracted from the existing land-cover classification, yielding 110 000 points for 11 NLCD classes. Urban classes were excluded, because they are derived from the percent impervious-surface data layer. Points common to all image pairs were used for classification in decision trees, with cross validation and boosting options in See5.

The cross validations of land cover indicated that a consistently more complex decision tree was generated with L5 data than with P6 AWiFS and LISS-III. This is likely caused by the presence of more spectral content (bands 1 and 7) in the Landsat data, and thus, more information available for decision-tree training.

Table V summarizes the mean-error estimates of each classification. The difference values show that L5 has lower estimated error than P6 AWiFS and LISS-III, most likely because of the presence of more spectral content in the L5 data. The large magnitudes of estimated error are not representative of the normal NLCD procedures, for reasons stated above, but the magnitudes of the estimated error differences between the two sensors range from 2% to 6%.

TABLE V
MEAN-ERROR ESTIMATES OF LAND-COVER CLASSIFICATIONS

Mean Error Estimates	
P6 AWiFS	44.9%
L5 TM	42.8%
Difference	2.1%
P6 LISS-III	50.7%
L5 TM	44.8%
Difference	5.9%

TABLE VI
LAND-COVER-CLASSIFICATION TEST

		P6 AWiFS	L5 TM	L5 TM –P6 AWiFS	P6 LISS-III	L5 TM	L5 TM –P6 LISS-III
	LC Class Name	% Correct	% Correct	delta %	% Correct	% Correct	delta %
1	open water	87.2	87.3	0.1	92.7	92.6	-0.2
2	barren land	86.3	87.1	0.7	76.2	81.9	5.7
3	deciduous forest	65.7	70.6	4.9	66.0	68.9	2.9
4	**evergreen forest**	**37.4**	**52.3**	**14.9**	**40.4**	**50.5**	**10.1**
5	mixed forest	69.4	68.8	-0.6	62.2	66.0	3.7
6	**shrub/scrub**	**39.7**	**46.6**	**6.9**	**36.0**	**44.5**	**8.4**
7	grassland	63.1	64.0	0.8	52.0	59.6	7.6
8	pasture/hay	29.6	30.6	0.9	22.5	26.4	3.9
9	cultivated crops	48.6	53.3	4.7	44.7	46.7	2.1
10	**woody wetlands**	**37.6**	**43.6**	**6.0**	**29.8**	**40.2**	**10.4**
11	**emergent wetlands**	**54.9**	**62.8**	**7.9**	**41.0**	**58.2**	**17.2**

TABLE VII
CROSS-VALIDATION STATISTICS FOR PERCENT TREE CANOPY TESTS

Canopy Estimates				
SLC, UT (L5 TM)	**P6 AWiFS**	**P6 LISS-III**	**L5 TM (vs. P6 AWiFS)**	**L5 TM (vs. P6 LISS-III)**
Average |error|	14.6	14.7	13.9	14.1
Relative |error|	0.58	0.58	0.55	0.56
Correlation coefficient	0.75	0.75	0.77	0.77
Mesa, AZ (L7 ETM+)	**P6 AWiFS**	**P6 LISS-III**	**L7 ETM+ (vs. P6 AWiFS)**	**L7 ETM+ (vs. P6 LISS-III)**
Average |error|	12.0	12.1	11.8	11.5
Relative |error|	0.70	0.67	0.69	0.64
Correlation coefficient	0.67	0.68	0.68	0.71

Table VI summarizes the 11 NLCD classes mapped by decision-tree methods. Overall, there are strong agreements in the ability to determine most classes, with differences of less than 5%.

For some classes (bolded text in the table), L5 was typically 5% or more accurate than P6 AWiFS and LISS-III. These occur on the classification of evergreen, shrub/scrub, woody wetlands, and emergent wetlands. Historically, L5 TM bands 1 and 7 have been widely used for vegetation and moisture discrimination, so increased difficulty with P6 AWiFS and LISS-IIII to classify moist and dry vegetation can be explained [15].

D. Canopy-Density Estimation

Tree-canopy density estimates are a continuous estimate of the percentage of tree cover, on a per-pixel basis. In this paper, they were generated by massively sampling approximately 1000 points per value, from 1 to 100 (totaling approximately 100 000) out of existing canopy products of both the Salt Lake City and Mesa sites. Points common to all image pairs were used for multiple regressions, using cross-validation and committee-model options.

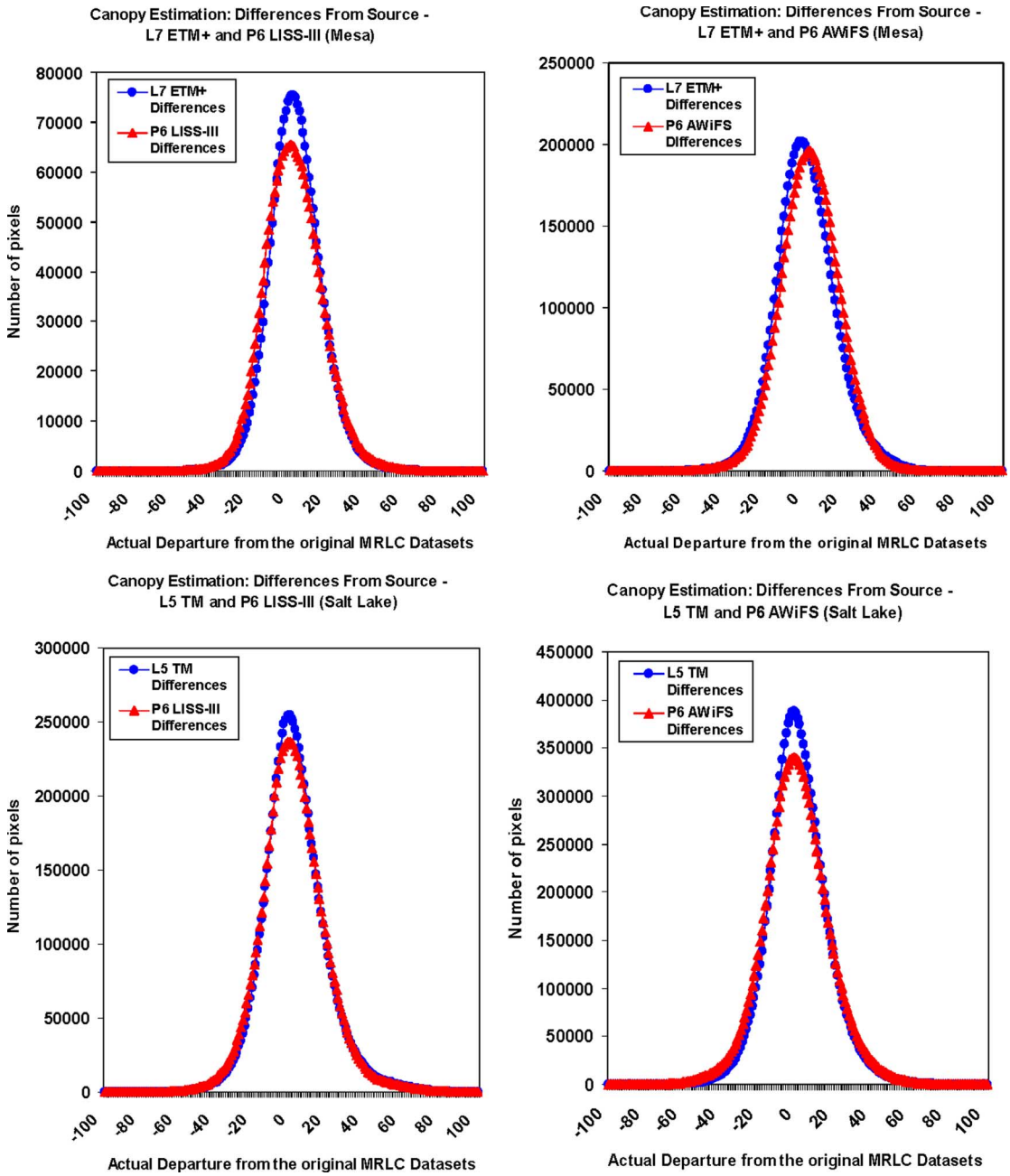

Fig. 15. Difference of percent tree canopy calculated from test imagery and NLCD 2001.

Table VII summarizes the percent tree canopy cross-validation results for both the Salt Lake City and Mesa test sites. The results typically show very slight (1%–2%) differences in average absolute error between L5 TM in Salt Lake City and L7 ETM+ in Mesa versus P6 AWiFS and LISS-III. Fig. 15 contains graphs of each percent-tree-canopy difference from the current NLCD 2001 standard product, where narrower bases and taller peaks imply closer agreement with the source. For the purpose of computing percent tree canopy, P6 AWiFS and LISS-III appear quite useful.

TABLE VIII
CROSS-VALIDATION STATISTICS FOR PERCENT IMPERVIOUS SURFACE TESTS

Impervious Estimates				
SLC, UT (L5 TM)	**P6 AWiFS**	**P6 LISS-III**	**L5 TM (vs. P6 AWiFS)**	**L5 TM (vs. P6 LISS-III)**
Average |error|	14.8	15.5	14.5	14.1
Relative |error|	0.59	0.61	0.58	0.56
Correlation coefficient	0.75	0.72	0.75	0.77
Mesa, AZ (L7 ETM+)	**P6 AWiFS**	**P6 LISS-III**	**L7 ETM+ (vs. P6 AWiFS)**	**L7 ETM+ (vs. P6 LISS-III)**
Average |error|	15.6	16.9	15.4	15.0
Relative |error|	0.65	0.78	0.64	0.70
Correlation coefficient	0.70	0.57	0.70	0.68

E. Impervious-Surface Estimation

Impervious-surface estimates are a continuous estimate of the percentage of impervious surface, on a per-pixel basis. In this paper, they were generated by massively sampling approximately 1000 points per value, from 1 to 100 (total approximately 100 000) out of existing impervious-surface products

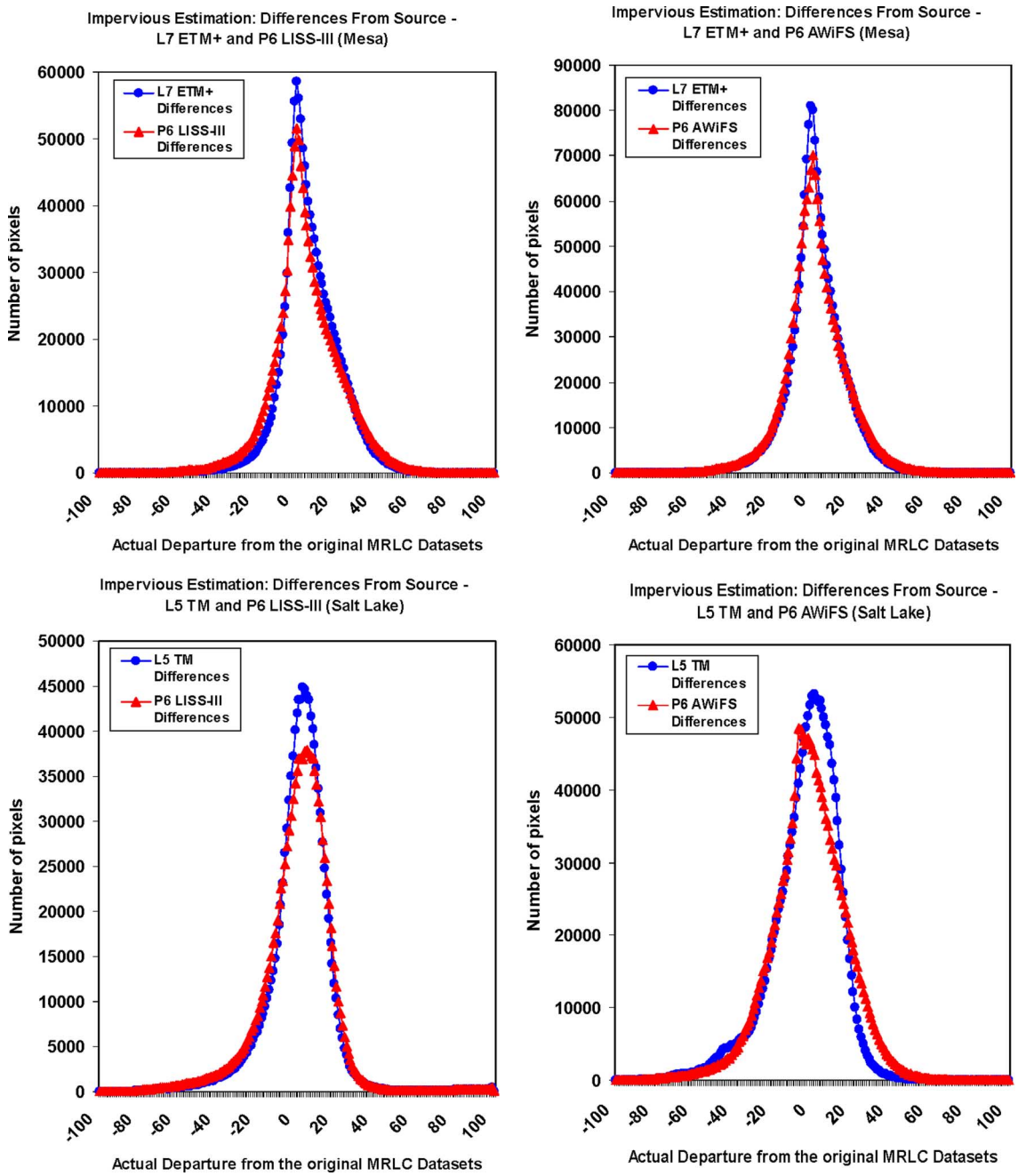

Fig. 16. Difference of percent impervious surface calculated from test imagery and NLCD 2001.

of both the Salt Lake City and Mesa sites. Points common to all image pairs were used for multiple regressions, using cross-validation and committee-model options.

Table VIII summarizes the impervious-surface cross-validation results for both the Salt Lake City and Mesa test sites. Similar to the canopy estimates, the results typically show very slight (1%–2%) differences in average absolute error between L5 TM in Salt Lake City and L7 ETM+ in Mesa versus P6 AWiFS and LISS-III. Fig. 16 contains graphs of each impervious estimate difference from the current NLCD standard product, where narrower bases and taller peaks imply closer agreement with the source. For the purpose of computing percent impervious surface, P6 AWiFS and LISS-III appear quite useful.

F. Further Discussions

Some anomalies were noted for both percent tree canopy and percent impervious surface data layers. For the Mesa site, the P6 AWiFS data were composed of all four quadrants, and intensity artifacts can be seen that were a result of the various quadrant overlaps (example in Fig. 17). A similar situation can be found in the L7 ETM+ mosaic of scan-gap data, with low intensity "stripes" (example in Fig. 18). Further work would be needed to identify an optimum method of using these data sets without generating these artifacts. The P6 LISS-III impervious estimate did not contain any artifacts and, therefore, may potentially outperform the L7 ETM+ scan-gap mosaic as a basis for tree canopy and impervious-surface estimates.

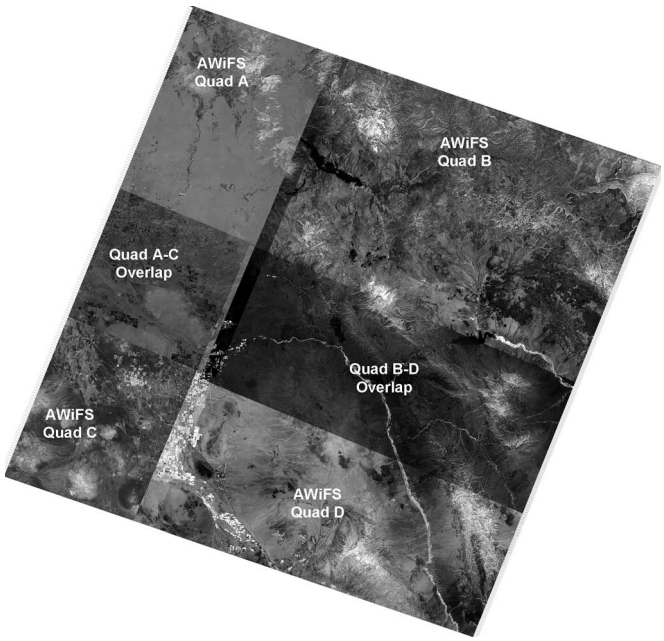

Fig. 17. Percent tree canopy map of AWiFS data over the extent of the Mesa, AZ, L7 ETM+ scene, showing the classification errors due to overlaps in the P6 AWiFS quadrants.

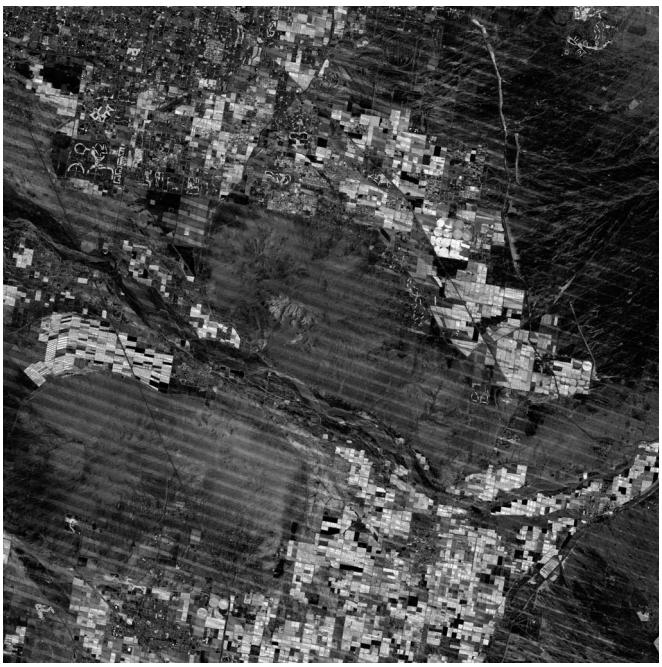

Fig. 18. Percent tree canopy map of L7 ETM+ data in part of the Mesa, AZ, scene, showing classification errors due to gap-filling.

V. Summary and Conclusion

To understand the absolute radiometric calibration accuracy of the P6 AWiFS and LISS-III sensors, image pairs from these sensors were compared to images from the L5 TM and L7 ETM+ sensors. The approach involved calibration of surface observations based on image statistics from areas observed nearly simultaneously by the two sensors. The average reflectance estimates obtained from these sensors agree within 13%.

This paper also provides an initial evaluation of the viability of the P6 platform for providing images suitable for generating three NLCD products: land cover, percent tree canopy, and percent impervious surface. Individual P6 AWiFS and LISS-III products were slightly less accurate in classifying particular land-cover classes but provided a very useful approximation to L5 TM and L7 ETM+ for percent tree canopy and percent impervious surface. Artifacts were noted in the areas of overlap, both of the P6 AWiFS quadrants and of the scan-gap L7 ETM+ mosaic. These drawbacks may be addressed by potential five-day revisits of the P6. More image acquisitions would be needed to investigate these issues.

Acknowledgment

The authors would like to thank J. Lutes (GeoEye), K. Kumar (ISRO), and S. Kumar (ISRO) for information and feedback. Any use of trade, product, or firm names is for descriptive purposes only and does not imply endorsement by the U.S. Government.

References

[1] *Landsat-7 Science Data User's Handbook*, (2006, Feb. 28). Greenbelt, MD: NASA Goddard Space Flight Center. [Online]. Available: http://ltpwww.gsfc.nasa.gov/IAS/handbook/handbook_toc.html

[2] *IRS-P6 Users Handbook*, (2003, Oct.). Hyderabad, India: NRSA. [Online]. Available: http://www.nrsa.gov.in/index.html

[3] J. Lutes, "Resourcesat-1 geometric accuracy assessment," in *Proc. ASPRS Annu. Conf.*, Baltimore, MD, Mar. 7–11, 2005. [CD-ROM].

[4] *Resourcesat-1 Orbit and Coverage Details*, Dulles, VA: GeoEye. [Online]. Available: http://www.geoeye.com/products/imagery/irs/resourcesat/technical_overview.htm

[5] G. Chander and B. L. Markham, "Revised Landsat-5 TM radiometric calibration procedures, and postcalibration dynamic ranges," *IEEE Trans. Geosci. Remote Sens.*, vol. 41, no. 11, pp. 2674–2677, Nov. 2003.

[6] G. Chander, B. L. Markham, and J. A. Barsi, "Revised Landsat-5 Thematic Mapper radiometric calibration," *IEEE Trans. Geosci. Remote Sens.*, vol. 4, no. 3, pp. 490–494, Jul. 2007.

[7] G. Chander, D. J. Meyer, and D. L. Helder, "Cross-calibration of the Landsat-7 ETM+ and EO-1 ALI sensors," *IEEE Trans. Geosci. Remote Sens.*, vol. 42, no. 12, pp. 2821–2831, Dec. 2004.

[8] P. M. Teillet, J. L. Barker, B. L. Markham, R. R. Irish, G. Fedosejevs, and J. C. Storey, "Radiometric cross-calibration of the Landsat-7 ETM+ and Landsat-5 TM sensors based on tandem data sets," *Remote Sens. Environ.*, vol. 78, no. 1/2, pp. 39–54, 2001.

[9] G. Chander and P. L. Scaramuzza, "Cross calibration of the Landsat-7 ETM+ and Landsat-5 TM with the Resourcesat-1 (IRS-P6) AWiFS and LISS-III sensors," in *Proc. SPIE Int. Symp.,* Goa, India, 2006, vol. 6407, pp. 640 70E.

[10] G. Chander, D. L. Helder, B. L. Markham, J. Dewald, E. Kaita, K. J. Thome, E. Micijevic, and T. A. Ruggles, "Landsat-5 TM on-orbit absolute radiometric performance," *IEEE Trans. Geosci. Remote Sens.*, vol. 42, no. 12, pp. 2747–2760, Dec. 2004.

[11] G. Chander, B. L. Markham, E. Micijevic, P. M. Teillet, and D. L. Helder, "Improvement in absolute calibration accuracy of Landsat-5 with Landsat-7 ETM+ data," in *Proc. SPIE Int. Symp.*, San Diego, CA, 2005, vol. 5882, pp. 588 209.1–588 209.12.

[12] *Multi-Resolution Land Characteristics Consortium Homepage*. [Online]. Available: http://www.mrlc.gov/

[13] C. Homer, C. Huang, L. Yang, B. Wylie, and M. Coan, "Development of a 2001 national land-cover database for the United States," *Photogramm. Eng. Remote Sens.*, vol. 70, no. 7, pp. 829–840, Jul. 2004.

[14] C. Homer, J. Dewitz, J. Fry, M. Coan, N. Hossain, C. Larson, N. Herold, A. McKerrow, J. N. VanDriel, and J. Wickham, "Completion of the 2001 national land cover database for the conterminous United States," *Photogramm. Eng. Remote Sens.*, vol. 73, no. 4, pp. 337–341, Apr. 2007.

[15] T. M. Lillesand and R. W. Kiefer, *Remote Sensing and Image Interpretation*, 3rd ed. New York: Wiley, 1994.

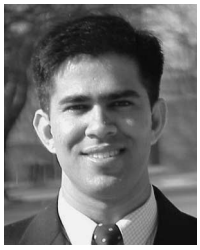

Gyanesh Chander (M'02) received the M.S. degree in electrical engineering from South Dakota State University, Brookings, in 2001.

He is currently a Senior Systems Engineer with Science Application International Corporation (SAIC), San Diego, CA, contractor to the U.S. Geological Survey (USGS) Center for Earth Resource Observation and Science (EROS), Sioux Falls, SD. For the past seven years, he has been working extensively with the National Aeronautics and Space Administration's Goddard Space Flight Center and the Stennis Space Center in the area of radiometric characterization and calibration of satellites and airborne sensors. He has been involved in the development of the Landsat-5 Thematic Mapper image assessment system and the EO-1 Advanced Land Imager image assessment system.

Mr. Chander is currently a member of the International Committee of Earth Observation Satellites and actively participates in the Working Group Calibration Validation and Infrared Visible and Optical Sensor's subcommittee meetings.

Michael J. Coan received the B.S. and M.S. degrees in spatial information and science from the University of Maine, Orono, in 1994 and 1996, respectively. His M.S. degree studies emphasized the use of remote sensing for monitoring natural resources.

He is currently a senior scientist with Science Application International Corporation (SAIC), San Diego, CA, contractor to the U.S. Geological Survey (USGS) Center for Earth Resource Observation and Science (EROS), Sioux Falls, SD. He has specialized in land-cover classifications with remote-sensing data and has actively contributed to the methodologies implemented in the various products of the USGS National Land Cover Database.

Pasquale L. Scaramuzza received the B.S. degree in physics from Drexel University, Philadelphia, PA, in 1990 and the M.S. degree in physics from Temple University, Philadelphia, in 1993.

He is currently a Radiometric Analyst with Science Application International Corporation (SAIC), San Diego, CA, contractor to the U.S. Geological Survey (USGS) Center for Earth Resource Observation and Science (EROS), Sioux Falls, SD, working on the Landsat-7 image-assessment system, where he performs the daily checks of the data and instrument calibrations, performs analyses on the radiometric performance of the instrument, and updates calibration parameters.